Molecular Recognition between Oligopeptides and Nucleic Acids: Sequence-Specific Binding of the Naturally Occurring Antibiotic (4S)-(+)-Anthelvencin A and Its (4R)-(-) Enantiomer to Deoxyribonucleic Acids Deduced from ^{1}H NMR, Footprinting, and Thermodynamic Data

Moses Lee,[†] Regan G. Shea,[†] John A. Hartley,[†] Koren Kissinger,[‡] Richard T. Pon,[§] Gorazd Vesnaver,[∥] Kenneth J. Breslauer,[∥] James C. Dabrowiak,[‡] and J. William Lown*,[†]

Contribution from the Department of Chemistry, University of Alberta, Edmonton, Alberta, Canada, T6G 2G2, Department of Chemistry, Syracuse University, Syracuse, New York 13120, Regional DNA Synthesis Laboratory, University of Calgary, Calgary, Alberta, Canada, T2N 4N1, and Department of Chemistry, Rutgers University, New Brunswick, New Jersey 08903. *Received March 21, 1988*

Abstract: The DNA sequence specificity of both the natural antibiotic (4*S*)-(+)-anthelvencin A (**1a**) and its unnatural (4*R*)-(-) enantiomer **1b** was determined by DNase I footprinting to be similar to that of netropsin. Structural and dynamic aspects of the binding of **1a** and **1b** to the double-helical decadeoxyribonucleotide d(CGCAATTGCG)$_2$ were studied by high-field ^{1}H NMR spectroscopy. The drug-induced chemical shifts and NOE measurements of the 1:1 complexes of (4*S*)-(+)-**1a** and (4*R*)-(-)-**1b** to the decadeoxyribonucleotide (complexes A and B, respectively) reveal that both enantiomeric forms of anthelvencin A bind in the minor groove along the sequence 5′-$A_4A_5T_6T_7$-3′ of the DNA. NOE studies show that the (4*S*) enantiomer **1a** is propeller twisted between the two pyrrole moieties to provide the structural flexibility for the drug to bind tightly in the minor groove along the 5′-AATT sequence on the DNA in complex A. In contrast, the unnatural (4*R*) enantiomer **1b** adopts a coplanar conformation in complex B. From molecular modeling studies, it is shown that the (4*S*) hydrogen of **1a** is directed out of the minor groove thereby positioning the positively charged 2-amino-1-pyrrolinium moiety for more favorable electrostatic interaction between the drug and DNA. Conversely, for (4*R*)-**1b** of complex B, the positively charged 2-amino-1-pyrrolinium group is directed out of the minor groove, and as a result, the interaction of this group with the negative potential of that section of the DNA is restricted. The natural (4*S*) enantiomer **1a** is not bound centrally between the d[($A_4A_5T_6T_7$)·($A_4A_5T_6T_7$)] DNA duplex but is located diagonally across the 5′-AATT base pair sequence. In contrast, the unnatural (4*R*) enantiomer **1b** behaves like achiral lexitropsins and binds centrally in the minor groove at the 5′-AATT base pair sequence. The rate of exchange of the chiral lexitropsins between equivalent sites is found to be dependent on the chirality of the oligopeptides. The exchange rates of (4*S*)-**1a** and (4*R*)-**1b** between the two equivalent 5′-AATT sites via the intramolecular flip-flop mechanism are $\sim$36 s^{-1} at 21 °C with $\Delta G^{\ddagger}$ of 68.3 ± 5 kJ mol^{-1} and $\sim$77 s^{-1} at 21 °C with $\Delta G^{\ddagger}$ of 62.5 ± 5 kJ mol^{-1}, respectively. Spectroscopic and calorimetric studies reveal that compounds (4*S*)-**1a** and (4*R*)-**1b** exhibit similar binding affinities for the poly[d(AT)]·poly[d(AT)] duplex, with $\Delta G°$ values of -33.5 and -33.0 kJ/mol, respectively, at 25 °C. Thus, the stereochemical difference between the enantiomers does not alter significantly the binding affinities of the two ligands for the poly[d(AT)]·poly[d(AT)] duplex. Furthermore, at 25 °C, the binding of both enantiomers to poly[d(AT)]·poly[d(AT)] is strongly entropy driven while the corresponding binding of the structurally similar ligand netropsin is strongly enthalpy driven. These results suggest that relatively small changes in drug structure can cause dramatic changes in the binding thermodynamics. The binding constants for both enantiomers exhibit very similar salt dependencies. Thus, the difference in chirality between the enantiomers does not alter the overall electrostatic contribution to the binding of the two ligands to the poly[d(AT)]·poly[d(AT)] duplex. Furthermore, the magnitude of the salt dependence of the binding constants for both enantiomers is characteristic of monocationic binding despite their formal dicationic structures. CD titration curves reveal that both anthelvencin enantiomers exhibit saturation binding site sizes equivalent to two base pairs. A model is proposed for the saturation binding of the two anthelvencins to the poly[d(AT)]·poly[d(AT)] duplex that is consistent with both the monocationic binding behavior and the binding site size. Collectively the data suggest the anthelvencins have one cationic terminus strongly bound to the minor groove site while the other terminus is less strongly bound.

There is continuing interest in the examination of the structure and conformation of oligopeptide–oligonucleotide complexes in solution and especially of the sequence dependence as it relates to the operation of gene control and expression.[1] The advent of efficient methods of DNA synthesis and newer two-dimensional NMR methods have permitted detailed studies on nucleic acid–oligopeptide complexes in solution to be undertaken.[2-7] NMR studies have revealed detailed information on the sequence-dependent interactions between the oligopeptides and DNA, as well as the dynamics of the complexes, in solution.[2-7]

The natural antitumor antibiotic oligopeptides netropsin and distamycin have received much attention as models of nonintercalative, minor groove, and sequence-specific DNA binding agents.[8-10] These agents exert their biological activities by blocking the template function of DNA by binding to $(A·T)_4$ and $(A·T)_5$ sequences, respectively.[8] Physical studies including X-ray

[†] University of Alberta.
[‡] Syracuse University.
[§] University of Calgary.
[∥] Rutgers University.

(1) (a) Caruthers, M. H. *Acc. Chem. Res.* **1980**, *13*, 155. (b) Frederick, C. A.; Grable, J.; Melia, M.; Samudzi, C.; Jen-Jacobson, L.; Wang, B. C.; Greene, P.; Boyer, H. W.; Rosenberg, J. W. *Nature (London)* **1984**, *309*, 327. (c) Gurskii, G. V.; Tumanyan, V. G.; Zavedatelev, A. S.; Zhyze, A. L.; Grokhovsky, S. L.; Gottikh, B. P. In *Nucleic Acid–Protein Recognition*; Vogel, H. J., Ed.; Academic: New York, 1977; p 189. (d) Kim, S. H.; Sussman, J. L.; Church, G. M. In *Structure and Conformation of Nucleic Acids and Protein–Nucleic Acid Interactions*; Sundaralingam, M., Rao, S. T., Eds.; University Park: Baltimore, MD, 1974; pp 571–575. (e) Takeda, Y.; Ohlendorf, D. H.; Anderson, W. F.; Matthews, B. W. *Science (Washington, D.C.)* **1983**, *221*, 1020.

(2) (a) Patel, D. J. *Proc. Natl. Acad. Sci. U.S.A.* **1982**, *79*, 6424. (b) Patel, D. J.; Shapiro, L. *J. Biol. Chem.* **1986**, *261*, 1230. (c) Pardi, A.; Morden, K. M.; Patel, D. J.; Tinoco, I., Jr. *Biochemistry* **1983**, *22*, 1107.

(3) Klevit, R. E.; Wemmer, D. E.; Reid, B. R. *Biochemistry* **1986**, *25*, 3296.

(4) (a) Sarma, M. H.; Gupta, G.; Sarma, R. H. *J. Biomol. Struct. Dyn.* **1984**, *1*, 1457. (b) Sarma, M. H.; Gupta, G.; Sarma, R. H. *J. Biomol. Struct. Dyn.* **1985**, *2*, 1085.

0002-7863/89/1511-0345$01.50/0

analysis of a complex of netropsin and d-$(CGCGAATT^{Br}CGCG)_2$[11,12] and ^1H NMR[2-7] and CD studies[13] have provided some structural details on the nature of the interactions between such information-reading oligopeptides, or lexitropsins, and DNA that contribute to their marked specificity. It has been shown that replacement of the pyrrole unit(s) and the guanidinium acetyl groups in netropsin with imidazole and formyl groups, respectively, can alter the recognition properties from dA·dT to dG·dC base pairs in a predictable fashion.[14-16] The rationale behind these modifications is that the introduction of hydrogen bond accepting heterocycles, such as imidazole, permits the recognition of dG·dC sites by the formation of new hydrogen bonds between the guanine-2-NH_2 and imidazole-N3 moieties.[14,15] This modification together with a reduction in cationic charge and removal of certain van der Waals contacts yields ligands that can target dG·dC sites. The recently prepared netropsin analogue, formyl-imidazole-imidazole-CH_2CH_2-amidine has been shown by DNase I footprinting on the *Hind*III/*Nci*I restriction fragment from pBR322 DNA to be specific for the sequence 5′-CCGT-3′.[16] ^1H NMR analysis of this compound in the presence of the duplex $d(CATGGCCATG)_2$ indicates that it binds preferentially to the sequence 5′-CCAT-3′.[17]

Thus far, none of the biophysical studies in our groups have been performed with oligopeptides containing chiral centers. This paper examines and interprets the influence of the chiral center of anthelvencin A on the sequence-specific molecular recognition of DNA. Therefore, we report the results on the sequence specificity of (4*S*)-(+)-**1a** and (4*R*)-(−)-**1b** determined by DNase I footprinting analyses. Furthermore, detailed ^1H NMR analyses on the structure and dynamics of the 1:1 complexes of (4*S*)-(+)-anthelvencin A (**1a**) and $d(CGCAATTGCG)_2$ (complex A) as well as the unnatural isomer (4*R*)-(−)-**1b** and the same decadeoxyribonucleotide (complex B) are also reported. Nuclear Overhauser effects between spatially separated protons have been especially valuable in providing information on interproton distances between the drug and the DNA in the drug–DNA complexes. Corroborating thermodynamic data on the binding of these compounds deduced from microcalorimetry are reported. Collectively the data have provided a model for the binding of anthelvencin to DNA.

Experimental Section

Chemicals and Biochemicals. The synthesis of both enantiomers of anthelvencin A [(4*S*)-(+)-**1a** and (4*R*)-(−)-**1b**] have been described.[18] The enantiomeric excess of **1a** and **1b** is determined to be 80 ± 4%.[18]

The DNA polymers used as host duplexes in this work were purchased from Pharmacia P.L. Biochemicals (Piscataway, NJ). The oligomer $d(CGCAATTGCG)_2$ was synthesized as described previously.[5] Each compound was obtained in dried form and was used without further purification. Solution concentrations were determined spectrophotometrically by using the following extinction coefficient, $\epsilon_{260} = 6650\ M^{-1}\ cm^{-1}$ for poly[d(AT)].

^1H NMR Studies. The NMR sample of the 1:1 complex of (4*S*)-(+)-**1a** and the decadeoxyribonucleotide $d(CGCAATTGCG)_2$ (complex A) was prepared by dissolving the DNA (8.9 mg) in a 99.8% D_2O solution (0.4 mL) containing 30 mM potassium phosphate (pH 7.2), 10 mM NaCl, and 0.1 mM EDTA. The sample was lyophilized once from 99.96% D_2O and finally redissolved in 99.96% D_2O (0.4 mL). A fresh stock solution of (4*S*)-(+)-**1a** in a 99.996% D_2O solution was prepared immediately before the titration experiment. For the 1:1 molar ratio of complex A, the concentration of the complex was 6.9 mM. For the 1:1 of (4*R*)-(−)-**1b** and $d(CGCAATTCGC)_2$ (complex B), the sample was prepared exactly as in the procedure given above, and the concentration of complex B was also 6.9 mM. For the detection of the exchangeable ^1H NMR signals, the sample was prepared in a 9:1 (v/v) H_2O/D_2O solution.

^1H NMR spectra were obtained at 21 °C on Bruker WM-360 and WH-400 cryospectrometers, both of which are interfaced with Aspect 2000 computers. The COSY[19] and NOESY[20] spectra were symmetrized but not apodized. The COSY, NOESY, and 1D-NOE difference[21] experiments were performed as described in our previous studies.[5-7,17] The experimental conditions used for the NMR experiments are given in the figure legends.

In detecting the exchangeable proton NMR signals, the binomial $1\text{-}\bar{3}\text{-}3\text{-}\bar{1}$ pulse sequence was used to suppress the intense HDO signal.[22] Complete assignments for the exchangeable and nonexchangeable ^1H NMR signals of $d(CGCAATTGCG)_2$ have been reported.[5]

DNase I Footprinting. Concentrations of both (4*S*)-(+)-**1a** and (4*R*)-(−)-**1b** were determined optically by using 292 nm, $\epsilon = 10.2\ mM^{-1}\ cm^{-1}$. The *Hind*III/*Nci*I 139 base pair restriction fragment from pBR322 DNA was isolated and 3′-end-labeled at position 33 of this fragment as previously described.[23] The buffer used for the footprinting digests involving DNase I was 37 mM Tris-HCl, pH 7.5, containing 2 mM $CaCl_2$ and 8 mM $MgCl_2$. After equilibration of the compounds with DNA, the enzyme was added and the reactions were carried out at 37 °C for 10 min. The total volume of each reaction was 8 μL, which contained as final concentrations 194 μM (base pairs) sonicated calf thymus DNA, ~1 μM (base pairs) labeled fragment, a specific concentration of either (4*S*)-**1a** or (4*R*)-**1b** and ~0.2 μM DNase I. The reaction products, the result of "single hit" kinetics, were separated with a field gradient electrophoresis device and visualized by autoradiography with Kodak X-O Mat Ar X-ray film. The autoradiographic data were scanned with a linear scanning microdensitometer/computer system.[23b] The numbering system used is the genomic system for pBR322 DNA.[23c]

Molecular Modeling. The computer-generated depictions of complexes A and B were obtained on a Zenith Z-158 microcomputer (Zenith Data Systems, MI) using the molecular graphics program PC MODEL (Academic Press Inc., Toronto) and Arnott's coordinates for B-DNA.[24a]

UV Melting Curves. Absorbance versus temperature profiles of the drug-free and the drug-bound DNA duplex were measured with a thermoelectrically controlled Perkin-Elmer 575 programmable spectrophotometer interfaced to a Tektronic 4051 computer. A heating rate of 0.5 °C/min was employed while the temperature (T) and the absorbance (A) at 260 nm were recorded every 30 s. Differential melting curves ($\Delta A/\Delta T$ versus T) were derived from these data by taking the difference in absorbance every degree. The corresponding melting temperatures (T_m) were derived from these curves by previously described methods.[24b]

(5) Lee, M.; Chang, D.-K.; Hartley, J. A.; Pon, R. T.; Krowicki, K.; Lown, J. W. *Biochemistry* **1988**, *27*, 445.
(6) Lee, M.; Pon, R. T.; Krowicki, K.; Lown, J. W. *J. Biomol. Struct. Dyn.* **1988**, *5*, 939.
(7) Lee, M.; Coulter, D. M.; Pon, R. T.; Krowicki, K.; Lown, J. W. *J. Biomol. Struct. Dyn.* **1988**, *5*, 1059.
(8) (a) Zimmer, C. *Prog. Nucleic Acid Res. Mol. Biol.* **1975**, *15*, 285. (b) Zimmer, C.; Wähnert, U. *Prog. Biophys. Mol. Biol.* **1986**, *47*, 31.
(9) Hahn, F. E. In *Antibiotics III. Mechanism of Action of Antimicrobial and Antitumor Agents*; Corcoran, J. W., Hahn, F. E., Eds.; Springer-Verlag: New York, 1975; pp 79–100.
(10) Dervan, P. B. *Science (Washington, D.C.)* **1986**, *232*, 464.
(11) Kopka, M. L.; Yoon, C.; Goodsell, D.; Pjurra, P.; Dickerson, R. E. *J. Mol. Biol.* **1985**, *185*, 553.
(12) Kopka, M. L.; Yoon, C.; Goodsell, D.; Pjurra, P.; Dickerson, R. E. *Proc. Natl. Acad. Sci. U.S.A.* **1985**, *82*, 1376.
(13) (a) Zimmer, C. *Comments Mol. Cell Biophys.* **1983**, *1*, 399. (b) Zimmer, C. *Stud. Biophys.* **1972**, *31/32*, 447.
(14) Lown, J. W.; Krowicki, K.; Bhat, U. G.; Skorobogaty, A.; Ward, B.; Dabrowiak, J. C. *Biochemistry* **1986**, *25*, 7408.
(15) Krowicki, K.; Lown, J. W. *J. Org. Chem.* **1987**, *52*, 3493.
(16) Kissinger, K.; Krowicki, K.; Dabrowiak, J. C.; Lown, J. W. *Biochemistry* **1987**, *26*, 5590.
(17) Lee, M.; Hartley, J. A.; Pon, R. T.; Krowicki, K.; Lown, J. W. *Nucleic Acids Res.* **1988**, *16*, 665.
(18) Lee, M.; Coulter, D. M.; Lown, J. W. *J. Org. Chem.* **1988**, *53*, 1855. Note that this optical purity estimated from the chiral shift reagent corresponds to 90 ± 4% of (*S*) and 10 ± 4% of (*R*) isomer. The worst case is therefore an 86:14 stereoisomer ratio and the best case is a 94:6 ratio. Since the limits of ^1H NMR detection are ca. 4% and no signals assignable to the second isomer were detected in either complex A or B, this suggests an actual stereoisomer ratio closer to the 94:6 ratio wherein the contaminating isomer does not materially affect the spectroscopic or calorimetric studies.
(19) Aue, W. P.; Bartholdt, E.; Ernst, R. R. *J. Chem. Phys.* **1976**, *71*, 2229.
(20) Macura, S.; Ernst, R. R. *Mol. Phys.* **1980**, *41*, 95.
(21) (a) Noggle, J. H.; Schirmer, R. D. *The Nuclear Overhauser Effect: Chemical Applications*; Academic: New York, 1971. (b) Detailed discussion of the assignment of all of the proton signals is given in the supplementary material.
(22) Hore, P. J. *J. Magn. Reson.* **1983**, *55*, 283.
(23) (a) Lown, J. W.; Sondhi, S. M.; Ong, C.-W.; Skorobogaty, A.; Kishikawa, H.; Dabrowiak, J. C. *Biochemistry* **1986**, *25*, 511. (b) Dabrowiak, J. C.; Skorobogaty, A.; Rich, N.; Vary, C. P. H.; Vournakais, J. N. *Nucleic Acids Res.* **1986**, *14*, 489. (c) Maniatis, T.; Fritsch, E. T.; Sambrook, J. *Molecular Cloning. A Laboratory Manual.* Cold Spring Harbor Laboratory: Cold Spring Harbor, NY, 1982.

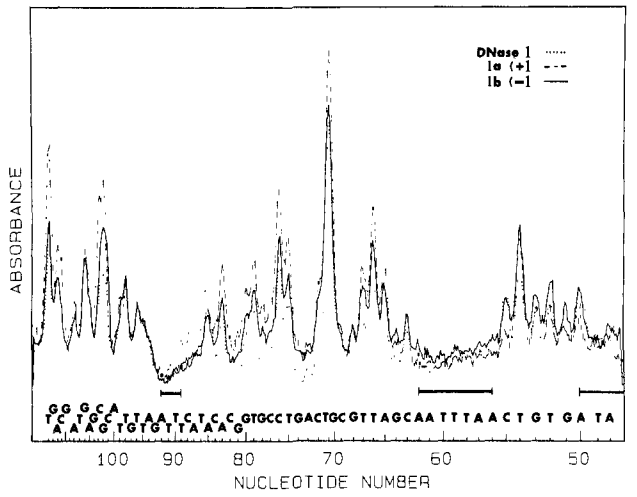

Figure 1. Densitometric scans of selected footprinting autoradiographic data for (4*S*)-(+)-**1a** (--) at 24.06 μM and (4*R*)-(−)-**1b** (—) at 24.06 μM. DNase I cleavage of the 139 base pair restriction fragment in the absence of ligand (···) is also shown. Primary binding sites of the ligands are indicated by bars below the scan.

Determination of Binding Constants, K_b, from UV Melting Curve Data. From the increase in the melting temperature of the ligand-bound duplex compared with the ligand-free duplex, we have obtained ΔT_m values for (4*S*)-**1a** and (4*R*)-**1b**. Following the theoretical treatment of Crothers,[24d] we used these ΔT_m values in conjunction with binding densities [determined from circular dichroism (CD) titration curves], transition enthalpies (determined by differential scanning calorimetry), and drug binding enthalpies (determined by batch calorimetry) to calculate binding constants, K_b.[24b] The details of this calculation have been described previously.[24b,f]

Determination of $\partial \log K_b/\partial \log [Na^+]$ Values. The "ΔT_m method" described above was used to calculate binding constants, K_b, over a range of salt concentrations. The resulting data were used to construct log–log plots of K_b versus $[Na^+]$. Such plots are linear with slopes ($\partial \log K_b/\partial \log [Na^+]$) that reflect the effective charge on the binding ligand.[24g,h] We used this approach to characterize the electrostatic contribution associated with the binding of (4*S*)-**1a** and (4*R*)-**1b** to the poly[d(AT)]·poly-[d(AT)] duplex.

Circular Dichroism (CD). All CD measurements were performed on an Aviv 60DS spectropolarimeter equipped with a thermoelectrically controlled cell holder. The binding of (4*S*)-**1a** and (4*R*)-**1b** to the poly[d(AT)]·poly[d(AT)] duplex was detected and monitored by measuring binding-induced changes in the optical properties of the bound ligand. Specifically, the binding-induced Cotton effect of the ligand near 310 nm provided a convenient optical window for following the binding process. CD titrations were performed by incrementally adding aliquots of each drug to CD cells containing known amounts of poly[d(AT)]·poly[d(AT)] and following the induced CD signal of each drug near 310 nm. The final spectra were normalized so that the CD titration profiles could be compared directly and used to establish binding curves. These binding curves were analyzed as previously described[24b] to yield the size of the binding site associated with each enantiomer.

Batch Calorimetry. The batch calorimeter used to determine the binding enthalpies reported here is based on the design of Prosen and Berger.[25a] The instrument previously has been described in detail.[24b,25b,c] The calorimeter was calibrated by using the heat of neutralization resulting from the reaction between a standardized solution of HCl and an excess of NaOH.

(24) (a) Arnott, S.; Campbell-Smith, P. J.; Chandrasakasan, R. In *Handbook of Biochemistry and Molecular Biology*; Fassman, O. D., Ed.; CRC: Cleveland, OH, 1976; p 411. (b) Marky, L. A.; Snyder, J. G.; Remeta, D. P.; Breslauer, K. J. *J. Biomol. Struct. Dyn.* **1983**, *1*, 487. (c) Marky, L. A.; Breslauer, K. J. *Biopolymers* **1987**, *26*, 1601. (d) Crothers, D. *Biopolymers* **1971**, *10*, 2147. (e) Marky, L. A.; Breslauer, K. J. *Proc. Natl. Acad. Sci. U.S.A.* **1987**, *84*, 4359. (f) Marky, L. A.; Curry, J.; Breslauer, K. J. In *Molecular Basis of Cancer, Part B, Macromolecular Recognition, Chemotherapy and Immunology*; Rein, R., Ed.; Alan R. Liss: New York, 1985; pp 155–173. (g) Manning, G. S. *Q. Rev. Biophys.* **1978**, *11*, 179. (h) Record, M. T.; Anderson, C. G.; Lohman, T. M. *Q. Rev. Biophys.* **1978**, *11*, 101.

(25) (a) Pennington, S. N.; Brown, H. D. In *Biochemical Microcalorimetry*; Brown, H. D., Ed.; Academic: New York, 1969; pp 207–219. (b) Mudd, C.; Berger, R. L.; Hopkins, H. P.; Friauf, W. S.; Gibson, C. *J. Biochem. Biophys. Methods* **1982**, *6*, 179. (c) Breslauer, K. J.; Charko, G.; Hrabar, D.; Oken, C. *Biophys. Chem.* **1978**, *8*, 393.

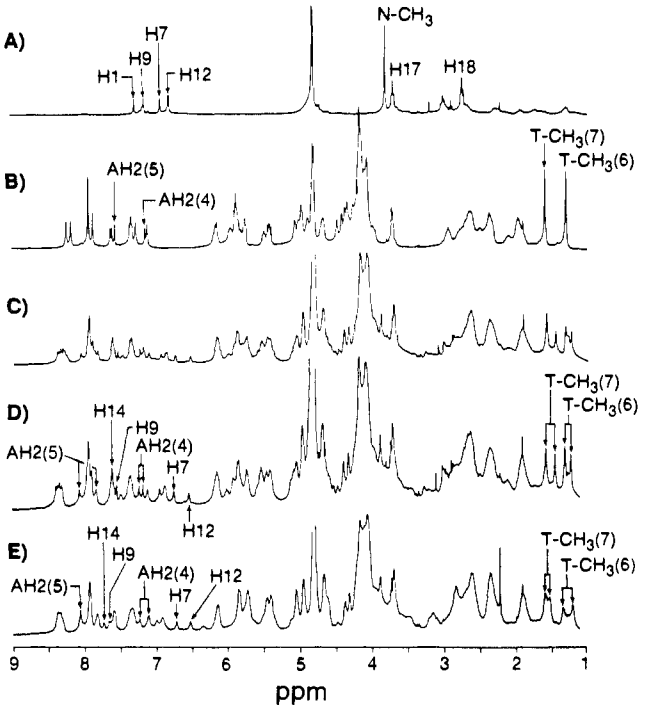

Figure 2. Titration of lexitropsin **1** to d(CGCAATTGCG)$_2$. Parts A and B correspond to the free lexitropsin and decadeoxyribonucleotide, respectively. Parts C and D represent the titration of 0.5 and 1.0 M equiv of (4*S*)-(+)-**1a** to the DNA. The NMR spectrum for the 1:1 complex of (4*R*)-(−)-**1b** to the decadeoxyribonucleotide is shown in part E.

Chart I. Structure and Numbering Systems of the Decadeoxyribonucleotide d(CGCAATTGCG)$_2$ and (4*S*)-(+)-Anthelvencin A (**1a**) and (4*R*)-(−)-**1b**.

A

d-C$_1$ G$_2$ C$_3$ A$_4$ A$_5$ T$_6$ T$_7$ G$_8$ C$_9$ G$_{10}$

I II III IV V V IV III II I

G$_{10}$ C$_9$ G$_8$ T$_7$ T$_6$ A$_5$ A$_4$ C$_3$ G$_2$ C$_1$-d

B

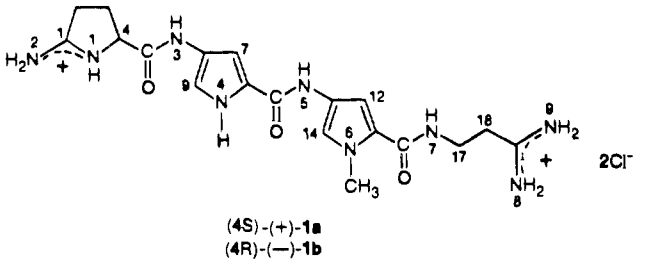

(4*S*)-(+)-**1a**
(4*R*)-(−)-**1b**

Results

DNase I Footprinting. The results of the DNase I footprinting experiments with (4*S*)-**1a** and (4*R*)-**1b** are shown in Figure 1. Both compounds bind with sequence specificity which is the same as that of netropsin.[14,26] The preference is for AT-rich sites with the sequences, all 5′ → 3′, ATAAA (50–46), AATTTAAC (62–56), and ATTT (92–89) showing the strongest binding. Secondary sites were also observed in the region flanking the AT tetramer at 92–89. These were all of the type (A·T)$_3$(G·C), i.e., CATTGTTAG (101–93) and CATAC (88–84). At identical ligand concentration both compounds exhibited comparable levels of inhibition.

^{1}H NMR Studies. The structure and numbering systems for the self-complementary decadeoxyribonucleotide d-(C$_1$G$_2$C$_3$A$_4$A$_5$T$_6$T$_7$G$_8$C$_9$G$_{10}$)$_2$ and anthelvencin A [(4*S*)-(+)-**1a** and (4*R*)-(−)-**1b**] are given in Chart I. In the DNA, the num-

(26) Ward, B.; Rehfuss, R.; Dabrowiak, J. C. *J. Biomol. Struct. Dyn.* **1987**, *4*, 685.

Table I. ^{1}H NMR Chemical Shift Assignments (ppm) of Nonexchangeable and Imino Protons of Complexes A and B in D_2O at 21 °C

		complex A		complex B	
base	DNA	δ	$\Delta\delta$	δ	$\Delta\delta$
CH6(1)	7.60	7.57	−0.03	7.60	0
GH8(2)	7.94	7.92	−0.02	7.94	0
CH6(3)	7.37	7.348 7.48	0.09	7.34	−0.03
AH2(4)	7.19	7.17, 7.22	~0.03	7.10, 7.23	~0.04
AH8(4)	8.26	8.32, 8.38	~0.12	8.33	0.07
AH2(5)	7.59	7.92, 8.06	~0.47	8.06	0.47
AH8(5)	8.20	8.29, 8.36	~0.16	8.30, 8.37	~0.17
TH6(6)	7.13	6.87, 6.94	~0.26	6.91, 6.99	~−0.22
T-CH_3(6)	1.29	1.23, 1.31	~−0.06	1.21, 1.34	~−0.08
TH6(7)	7.28	6.87, 7.11	~−0.41	6.99, 7.00	~−0.29
T-CH_3(7)	1.58	1.45, 1.57	~−0.13	1.53, 1.59	~−0.05
GH8(8)	7.88	7.83	−0.05	7.83	−0.05
CH6(9)	7.36	7.34	−0.02	7.34	−0.02
GH8(10)	7.95	7.92	−0.03	7.94	−0.01
		Imino Protons			
I C_1·G_{10}	12.88[a]	12.89	0.01	12.65	−0.23
II G_2·C_9	12.96	12.99	0.03	12.99	0.03
III C_3·G_8	12.58	12.65	0.07	12.53	−0.05
IV A_4·T_7	13.71	13.81, 14.09	~0.38	13.62, 14.12	~0.41
V A_5·T_6	13.58	13.63, 13.75	~0.17	13.36, 13.54	~−0.33
		Drug Protons			
NH3	10.52[b]	10.13, 10.35		9.70, 10.09	
NH5	10.09[b]	9.37		9.34	
NH7	8.37[b]	8.87		8.99	
H7	6.95	6.74	−0.21	6.73	−0.22
H9	7.17	7.54	0.37	7.66	0.49
H12	6.83	6.54	−0.29	6.53	−0.30
H14	7.30	7.62	0.32	7.75	0.45
N(6)-CH_3	3.80	3.87	0.07	3.89	0.09

[a] Determined at 4 °C. [b] Recorded in DMSO-d_6.

bering of the imino protons reflects the 2-fold symmetry observed for the solution conformation of the free duplex. The numbering system for **1** is adapted from that used in the crystallographic studies on netropsin.

Titration of (4*S*)-(+)-1a and (4*R*)-(−)-Anthelvencin A to d(CGCAATTGCG)$_2$ and Characterization of the Binding of 1a and 1b to the DNA. In Figure 2, the ^{1}H NMR spectra of the nonexchangeable protons of anthelvencin A and d(CGCAATTGCG)$_2$ are given in parts A and B, respectively. The results of the titration of (4*S*)-(+)-**1a** to the decadeoxyribonucleotide are given in Figure 2C,D with the former and latter spectrum representing the addition of 0.5 and 1 equiv of **1a**, respectively. The ^{1}H NMR spectrum of the 1:1 complex of (4*R*)-(−)-**1b** and the decadeoxyribonucleotide is depicted in Figure 2E.

With increasing proportions of (4*S*)-anthelvencin A (**1a**), resonances from the original decamer spectrum decrease and then disappear completely after the addition of 1.0 mol equiv (1:1 drug–DNA complex), while new resonances appear and increase in proportion to the amount of drug added (see Figure 2C,D). The effect is most evident for the methyl resonances of T(6,7) and many other aromatic base protons. The increased line width of the well-separated drug and DNA resonances in the low-field sections of the ^{1}H NMR spectra provides clear evidence for binding of **1a** and **1b** to the DNA. The broadening of NMR signals is probably due to the increase in the rotational correlation time[27] and the exchange process of the drug on the DNA. The spectra for complexes A and B, obtained at 21 °C, exhibit slow-exchange behavior (see Figure 2D,E). This is due to slow exchange of the drug between equivalent binding sites on the DNA on the NMR time scale, and as a result, the signals doubled. The appearance of exchange signals for AH8(4,5), AH2(4,5), TH6(6,7), and T-CH_3(6,7) (see Figure 2D,E) provides the first indication that both enantiomeric forms of anthelvencin A are located along the minor groove at the AATT sequence in the DNA.

Assignment of the Nonexchangeable ^{1}H NMR Resonances in Complexes A and B: Location and Orientation of the Drugs 1a and 1b on d(CGCAATTGCG)$_2$. The strategy used for assigning the nonexchangeable ^{1}H NMR resonances of the complexes is similar to that employed in our previous studies of oligopeptide–DNA complexes.[5-7,17] The ^{1}H NMR signals of complexes A and B were assigned by COSY,[19] NOESY,[20] and NOE difference[21a] techniques.

It is clear from the COSY spectrum of complex A (not shown) that the CH6(3) signal is doubled owing to the exchange of **1a** on the DNA. In addition to the CH5–CH6 correlations, the correlations for the lexitropsin H9–H12, H12–H14 signals of **1a** are also identified.

The results obtained from the NOE difference experiments for complex A are given in Figure 3 together with the reference spectrum in Figure 3A.[21b] It is established that AH2 signals in B-DNA have the longest T_1 relaxation time.[29] From the nonselective inversion recovery experiment performed on complex A at 21 °C (data not shown), the slowly relaxing signals for AH2a,b(5), AH2a,b(4) of the DNA and H7, H9, H12, and H14 of **1a** are observed. The pyrrole protons of **1a** are readily identified by the corresponding H7–H9 and H12–H14 correlations in the COSY spectrum. Saturation of the low-field pyrrole proton at 7.62 ppm gave NOE peaks at 6.54 and 3.87 ppm; therefore, these signals can be assigned to H14, H12, and N(6)-CH_3, respectively. Consequently, the signals at 7.54 and 6.74 ppm must belong to H9 and H7, respectively. The two sets of exchanging AH2 signals 8.06–7.92 and 7.22–7.17 ppm are identified from the NOE difference spectra (Figures 3C and 3F) and the NOESY spectrum which is discussed below. From the NOE difference spectra of the imino protons, the AH2 assignments are secured. Saturation of imino proton IV at 14.09 ppm gave a NOE peak at 7.17 ppm for AH2(4), while irradiation of imino proton V at 13.63 ppm produced a NOE signal at 8.06 ppm for AH2(5). The assignments of the nonexchangeable protons for complex A are summarized in Table I.

(27) James, T. L. *Nuclear Magnetic Resonance in Biochemistry*; Academic: New York, 1975; p 20.
(28) Debart, F.; Rayner, B.; Imbach, J.-L.; Chang, D. K.; Lown, J. W. *J. Biomol. Struct. Dyn.* **1986**, *4*, 343.
(29) Debart, F.; Rayner, B.; Imbach, J.-L.; Lee, M.; Chang, D. K.; Lown, J. W. *J. Biomol. Struct. Dyn.* **1987**, *5*, 47.

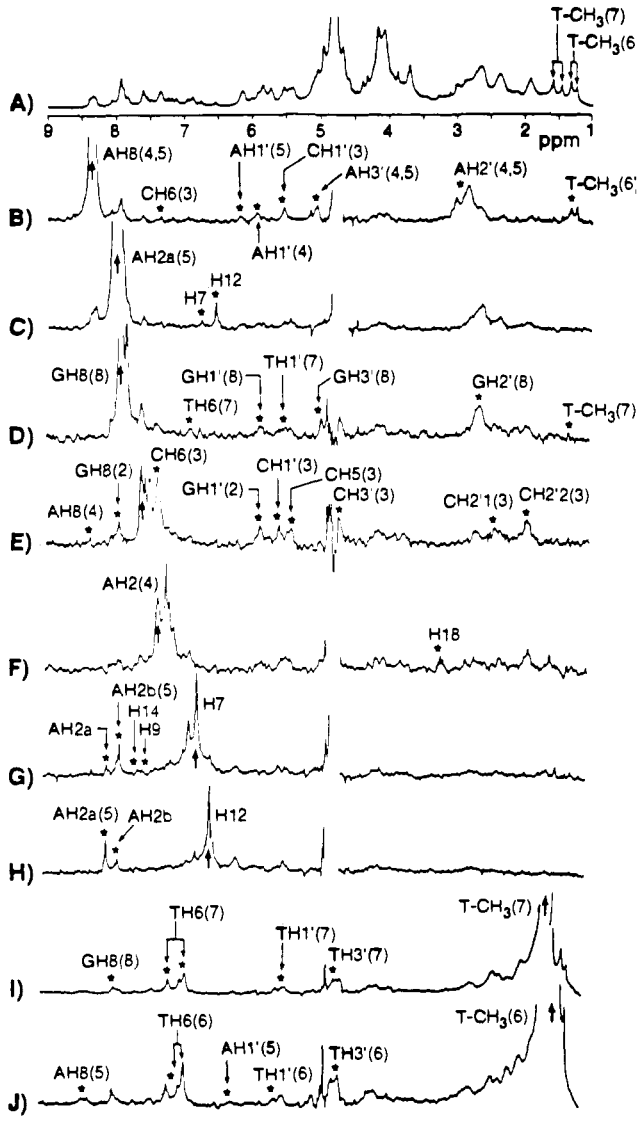

Figure 3. NOE difference spectra for complex A at 21 °C. Sweep width = 4000 Hz, irradiation time for NOE buildup = 0.4 s, and 800 FIDs were collected for each measurement. The arrows indicate the peaks saturated, and asterisks show the NOEs observed.

The nonexchangeable (Figure 2E) ^{1}H NMR signals of the 1:1 complex of (4*R*)-(−)-**1b** and d(CGCAATTGCG)$_2$ (or complex B) were assigned by using essentially the strategy discussed above. From the COSY spectrum (data not shown), the antibiotic H7–H9 and H12–H14 correlations of **1b** as well as the CH5–CH6 connectivities of the DNA are determined. Complete assignment of the nonexchangeable proton signals for complex B was achieved with the NOE difference spectra (data not shown).[30] The assignments of the nonexchangeable protons of complex B are given in Table I.

Assignment of the Exchangeable Protons of Complexes A and B. The DNA imino and antibiotic amide proton NMR spectra of complex A are given in Figure 4. These spectra were recorded in 9:1 (v/v) H_2OD_2O solutions at 294 K. Generally, the chemical shift of the imino proton of a dA·dT base pair resonates at lower field than that for a dG·dC base pair.[29] The ^{1}H NMR spectrum of the exchangeable protons of complex A reveals seven imino protons and four hydrogen-bonded amide protons, and the assignment for these signals is given in Figure 4.[21b] The exchangeable proton NMR signals of complex B (data not shown) were assigned by NOE difference measurements. The assignments

(30) All results listed as data not shown are available on request from the authors.

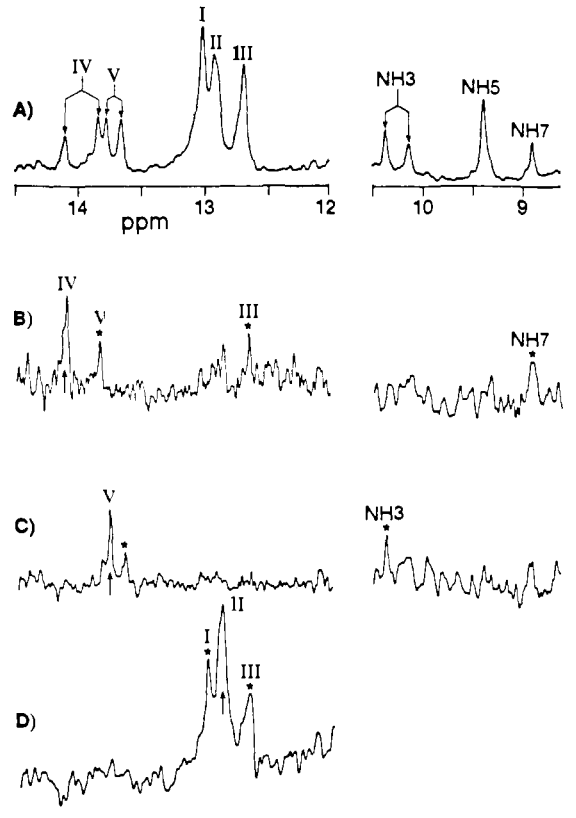

Figure 4. 1D-imino ^{1}H and NOE difference spectra of complex A in a 9:1 (v/v) H_2OD_2O solution at 21 °C. The binomial 1–3–3–1 pulse sequence was used for suppressing the HDO signal. Experimental conditions: spectral width = 8064 Hz, irradiation time = 0.4 s, and 320 FIDs were accumulated for each experiment.

of the imino and amide protons for complexes A and B are given in Table I.

All the imino proton resonances in complexes A and B are observable at 21 °C, while all the imino proton signals of free d(CGCAATTGCG)$_2$ can only be detected at or below 4 °C.[5] This result suggests that there is a kinetic stabilization of the DNA double helix not only to the binding site, $A_4A_5T_6T_7$, but also at the adjacent base pairs. The stabilization of the DNA double helix and increase in the lifetime for exchange of the imino protons in the DNA to the medium upon binding of netropsin have also been studied by ^{1}H NMR.[2c]

Location and Orientation of (4*S*)-(+)- and (4*R*)-(−)-Anthelvencins on d(CGCAATTGCG)$_2$ in Complexes A and B. The appearance of exchange signals for AH8(4,5), AH2(4,5), TH6(6,7), and T-CH$_3$(6,7) as illustrated in Figure 2D,E for complexes A and B, respectively, suggests that the antibiotic is located at the AATT sequence in the DNA for both the complexes. In addition, the marked drug-induced down-field shift and doubling of the resonances for imino proton IV and V provide support for the location of the drug at the AATT sequence on the DNA for both complexes.

The location of the ligand **1a** and **1b** on d(CGCAATTGCG)$_2$ is supported by chemical shift measurements. The ligand-induced chemical shift changes ($\Delta\delta$) of individual protons of the DNA duplex versus the decadeoxyribonucleotide for complexes A and B are plotted in Figure 5A,B, respectively. These graphs demonstrate that the base residues A(4)–T(7) are influenced most strongly by the binding of (4*S*)-(+)-**1a** and (4*R*)-(−)-**1b**. The results suggest that both enantiomeric forms of anthelvencin A, when challenged with d(CGCAATTGCG)$_2$, bind to the sequence AATT and are in accord with the excluded site size of four base pairs for the binding of netropsin to d(CGCGAATT^{Br}CGCG)$_2$ deduced by X-ray crystallographic studies.[11,12]

More direct identification of the intermolecular contacts was obtained from observation of NOEs between protons located in d(CGCAATTGCG)$_2$ and in **1a** and **1b**, respectively. The ade-

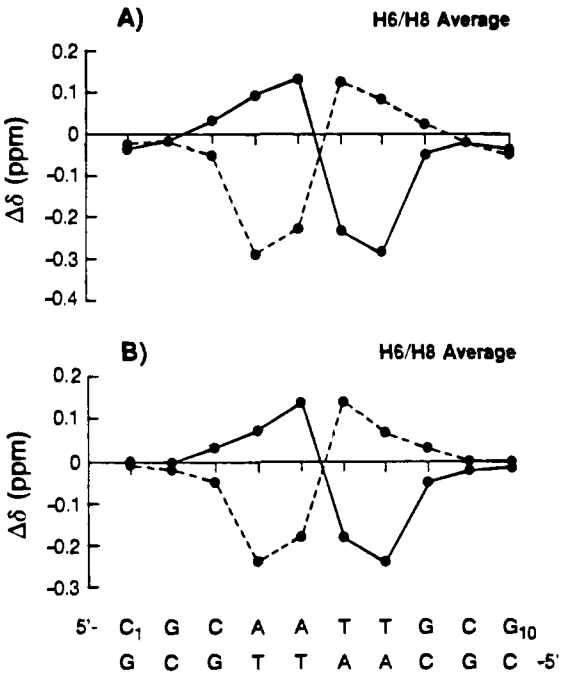

Figure 5. Graphical presentation of the drug-induced chemical shift changes for selected protons in the DNA sequence of complex A (part A) and complex B (part B). Positive values represent that the resonances in the 1:1 complex are at lower field than that in the free DNA. Both strands of the DNA are shown at the bottom, and the lexitropsin-induced chemical shift changes ($\Delta\delta$) for each of the two strands are drawn.

nine-H2 protons of base pairs 4 and 5 line the minor groove of the $d(A_4A_5T_6T_7)_2$ core of the decadeoxyribonucleotide duplex. The NOE method was applied to probe for intermolecular contacts between the adenine-H2 protons and protons of the antibiotic directed toward this groove. The AH2 signals of complexes A and B have been assigned as discussed earlier. It is noteworthy that the AH2(5) resonances of complexes A and B are markedly deshielded (~+0.40 and +0.47 ppm, respectively) as a result of drug binding. These results further support the location of the lexitropsin on the AATT sequence of the DNA for both complexes.

The partial NOESY spectrum of complex A is given in Figure 6A. The chemical exchange signals of AH2(4,5) can be seen in the spectrum. The loss of degeneracy can only arise as a result of drug binding wherein the two strands now have separate identities. As can be seen in Figure 6A, the NOESY correlations between AH2a(5) and H12 as well as AH2b(5) and H7 are labeled. These intermolecular contacts are confirmed by independent 1D-NOE studies (Figure 3C,G,H). If one assumes that the NOE buildup is still in the linear phase during the 0.4-s irradiation time used, the distances between AH2a(5)–H12 and AH2b(5)–H7 can be estimated.[31a] The measured cross-correlation rates [product of the steady-state NOE and spin–lattice relaxation, 2.16 s for AH2a(5) and AH2b(5)] can be used to derive the interproton distances of 3.10 Å for AH2a(5)–H12 and AH2b(5)–H7 and 4.10 Å for AH2a(5)–H7 and AH2b(5)–H12. These results suggest that the (4*S*)-(+) enantiomer **1a** is bound in the minor groove of the DNA along the sequence AATT and displaces the shell of hydration[11] by making similar hydrogen bonds

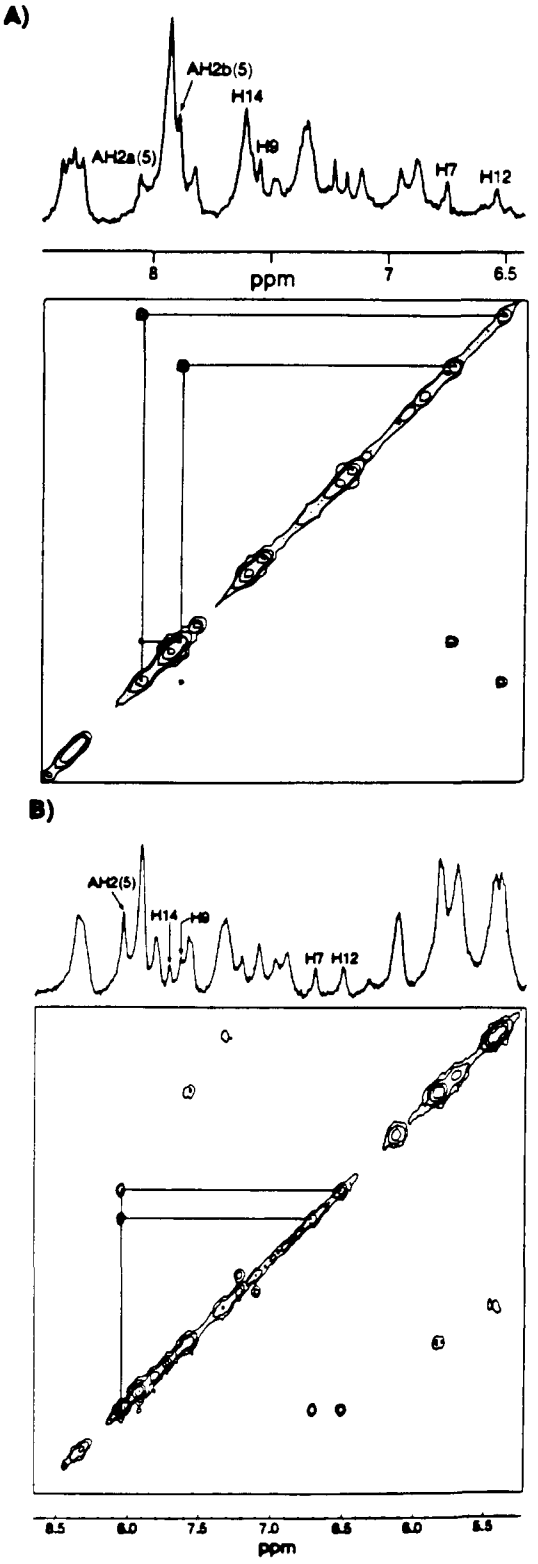

Figure 6. Expanded NOESY spectra of complex A (part A) and complex B (part B) at 21 °C. Experimental conditions: Part A, sweep width = 2941 Hz, initial t_1 = 3 μs, Δt_1 = 0.34 ms, recycle delay = 2.5 s, F_2 = 1K, and 32 FIDs were collected for each of the 256 experiments; part B, sweep width = 2702 Hz, initial t_1 = 3 μs, Δt_1 = 0.37 ms, RD = 2.5 s, and 64 FIDs were accumulated for each of the 256 experiments.

between the drug amide protons and the pyrine-N3 and pyrimidine-O2 groups.

The NOESY spectrum of complex B is given in Figure 6B. Strong NOEs between AH2(5) and H7 as well as H12 of the concave face of the lexitropsin are observed in the NOESY and NOE difference (data not shown) spectra. The distances between

(31) (a) Patel, D. J.; Kozlowski, S. A.; Bhatt, R. *Proc. Natl. Acad. Sci. U.S.A.* **1983**, *80*, 3908. (b) For complex A, the NOE observed between the exchanging signals of AH2(4) and H18 of **1a** (Figure 3F) provides evidence for the orientation of the drug in the 1:1 complex such that the amino to carboxyl termini of **1a** are bound to the 5′-$A_4A_5T_6T_7$-3′ reading from left to right. This is supported by the appearance of NOEs between imino proton IV and NH7 of **1a** (Figure 4B) and proton V and NH3 (Figure 4C). The results provide unambiguous evidence for the orientation of **1a** and the 5′-AATT-3′ of the DNA. A general model of the 1:1 complex of **1a** and the 5′-AATT-3′ duplex is given in Figure 7. The NOE observed between H18 of **1b** and the exchanging signals for AH2(4) (data not shown) indicates that the N to C termini of **1b** are also bound to the 5′-AATT-3′ sequence on the duplex DNA in the direction 5′ to 3′.

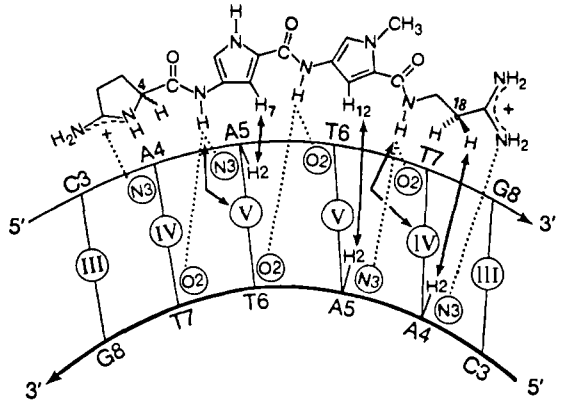

Figure 7. Alignment of lexitropsins (4*S*)-**1a** and (4*R*)-**1b** on the 5′-AATT-3′ base pair sequence on d(CGCAATTGCG)$_2$. Dotted lines represent hydrogen bonding between the drug amide and amidinium protons and purine-N3 and pyrimidine-O2 of the DNA. The intermolecular contacts between the protons on the concave face of the drug and protons in the minor groove of the 5′-AATT base pair sequence, determined from NOE studies, are illustrated with double-headed arrows.

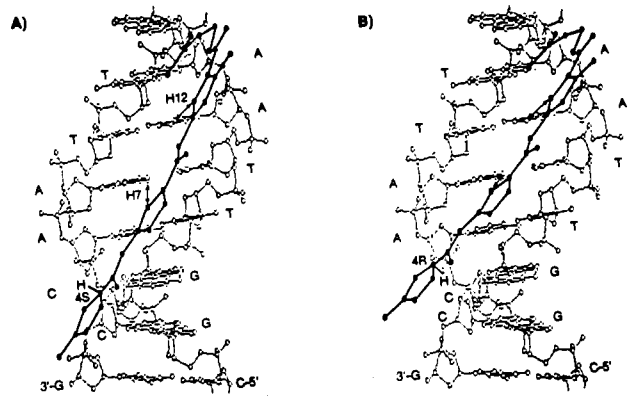

Figure 8. Computer-generated depiction of complex A (part A) and complex B (part B). The double-headed arrows represent the NOE observed between H7 and H12 of the drug and AH2(5) of the DNA. In part A, the (4*S*) hydrogen is pointing out of the minor groove, whereas in part B, the (4*R*) hydrogen is pointing into the minor groove.

AH2(5)–H12 and AH2(5)–H7 are estimated to be 3.52 Å. These results confirm the binding of (4*R*)-(−)-anthelvencin A (**1b**) in the minor groove of the DNA along the sequence AATT.[31b]

These results are consistent with the previous finding reported by us[32] that it is this van der Waals interaction between H18 of **1a** and **1b** and G-2-NH$_2$ that prevents the binding of the C terminus of the drugs to 3′-dG·dC sites, thus forcing the C terminus to read dA·dT sites.[32]

Positioning of the Anthelvencins and DNA in Complexes A and B. The conformation of the antibiotic in the complexes is determined by NOE studies. Saturation of the H7 signal of complex A, at 6.74 ppm, gave NOEs to H9 and H14 (Figure 3G), suggesting that natural drug (4*S*)-(+)-**1a** is propeller twisted between the two pyrrole moieties.

In contrast, no NOEs are observed between the two heterocyclic moieties of **1b** in complex B (data not shown). These results, in contrast to those of complex A, suggest that the unnatural drug (4*R*)-(−)-**1b** adopts a conformation in complex B that is closer to coplanar.

As mentioned earlier, both AH2 signals of A(4,5) of complex A are doubled, whereas only AH2(4) in complex B is doubled. The distance estimated between AH2a(5)–H7 and AH2b(5)–H12 is ~4.10 Å. Since AH2a(5) and AH2b(5) represent the two complementary strands of the DNA as a result of drug binding, these results suggest that the natural (4*S*)-(+) enantiomer **1a** is bound diagonally with respect to the AATT duplex, whereby H12 and H7 are close to AH2a(5) and AH2b(5), respectively. A computer-generated depiction of complex A is given in Figure 8A. The depictions in Figure 8A,B are given to provide the reader with three-dimensional structural representations of complexes A and B respectively, and they were generated without energy minimization. In complex A (Figure 8A), the hydrogen atom at the chiral center (4*S*) of **1a** is oriented out of the minor groove of the DNA. This would allow more favorable electrostatic interactions between the positively charged 2-amino-1-pyrrolinium group of **1a** and the DNA.

The distance between AH2(5)–H12 and AH2(5)–H7 in complex B is 3.52 Å. Since the AH2(5) resonances represent the two complementary strands of the DNA, this result indicates that the unnatural enantiomer (4*R*)-(−)-**1b** is bound centrally between the d[(A$_4$A$_5$T$_6$T$_7$)·(A$_4$A$_5$T$_6$T$_7$)] DNA duplex. A diagram of the complex is shown in Figure 8B. In this case, the hydrogen atom at the chiral center (4*R*) of **1b** is directed into the minor groove, thereby sterically diminishing the interactions between the positively charged 2-amino-1-pyrrolinium group of **1b** and the DNA.

The results indicate that the binding of the unnatural enantiomer (4*R*)-(−)-**1b** to the DNA is similar to that of achiral lexitropsins.[2] However, the natural enantiomer (4*S*)-(+)-**1a** binds to right-handed B-DNA in a unique manner whereby the drug molecule is bound snugly in the minor groove of the DNA and thereby allows hydrogen bonding, van der Waals contacts, and electrostatic interactions between these two molecules to take place more favorably. The difference in the binding properties of (4*S*)-**1a** and (4*R*)-**1b** to DNA is also reflected in the overall binding affinity of the drugs to calf thymus DNA determined by the ethidium displacement assay.[18,33]

The conformation of the oligonucleotide duplex can be determined by NOE measurements. The pattern of NOE intensities for AH8(4,5), GH8(8), and CH6(3) for complex A given in Figure 3 is in agreement with that of a right-handed B-DNA conformation.[34] This deduction is confirmed by the appearance of NOE peaks between AH8(4)–CH1′(3), GH8(8)–TH1′(7), and CH6(3)–GH1′(2) given in Figure 3B,D,E.[35] The conformation of the DNA duplex in complex B is also assigned to the B family.

Exchange Processes for Complexes A and B. From the nonexchangeable ^{1}H NMR and NOESY spectra of complexes A and B given in Figures 2D, 6A, and 2E, respectively, one can detect exchange signals for AH8(4,5), AH(4,5), TH6(6,7), and T-CH$_3$(6,7). The effect is most evident for the methyl resonances of T(6,7). Coalescence for T-CH$_3$(6) are observed at 50 and 30 °C for complexes A and B, respectively. Using the standard formula for two-site exchange with equal population,[36] the rate of exchange of **1a** between the two equivalent 5′-AATT sites on the decadeoxyribonucleotide in complex A is ~60 s^{-1} at 50 °C, with a $\Delta G^{\ddagger}$ of 68.3 ± 5 kJ mol^{-1}. In contrast, the rate of exchange of the unnatural epimer **1b** between the two equivalent 5′-AATT sites on the decamer is estimated to be ~104 s^{-1} at 30 °C, with $\Delta G^{\ddagger}$ of 62.5 ± 5 kJ mol^{-1}. At room temperature (21 °C), the exchange rate of **1a** in complex A and **1b** in complex B between the two equivalent binding sites are about 36 and 77 s^{-1}, respectively. These results are consistent with the aforementioned conclusion that the 5′-AATT-3′ sequence is better suited for the natural (4*S*)-(+) enantiomer **1a**, than its enantiomer (4*R*)-(−)-**1b**.

The flip-flop intramolecular exchange mechanism[3] (Figure 9) is the simplest to fit the experimental data for both complexes. The exchange of both enantiomeric forms of anthelvencin A

(32) Lee, M.; Krowicki, K.; Hartley, J. A.; Pon, R. T.; Lown, J. W. *J. Am. Chem. Soc.* **1988**, *110*, 3641.

(33) These studies are in accord with the previous investigation on the effects of the chiral centers of dihydroxybis(netropsin)succinamide on their binding affinity to DNA: Griffin, J. N.; Dervan, P. B. *J. Am. Chem. Soc.* **1986**, *108*, 5008. The authors suggest that the right-handed twist of (*S*,*S*)-dihydroxybis(netropsin)succinamide fits better in the minor groove of right-handed B-DNA than does the left-handed twist of the (*R*,*R*) enantiomer (vide infra). Therefore, the former ligand binds more strongly to DNA than the latter.

(34) Gronenborn, A. M.; Clore, G. M. *Prog. Nucl. Magn. Reson. Spectrosc.* **1985**, *17*, 1.

(35) Hare, D. R.; Wemmer, D. E.; Chou, S. H.; Drobny, G.; Reid, B. R. *J. Mol. Biol.* **1983**, *171*, 319.

(36) Dalling, D. K.; Grant, D. M.; Johnson, L. F. *J. Am. Chem. Soc.* **1971**, *93*, 3678.

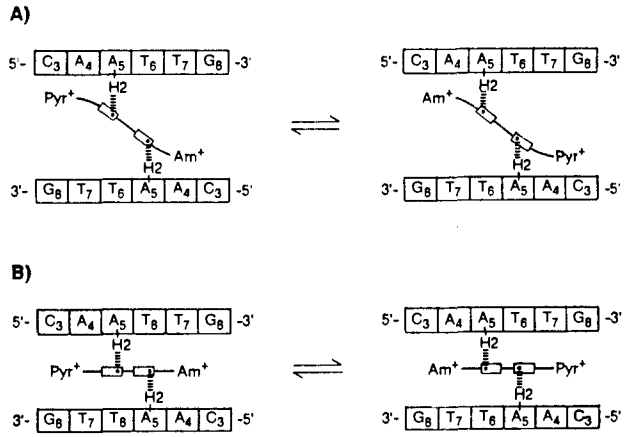

Figure 9. The intramolecualr flip-flop exchange mechanism of the drug between two equivalent 5′-AATT binding sites of the DNA for complex A (part A) and complex B (part B). It should be noted that the (4*S*)-(+) enantiomer **1a** is bound across the two strands of DNA in the d-[$(A_4A_5T_6T_7)\cdot(A_4A_5T_6T_7)$] duplex, whereas the unnatural (4*R*)-(−) enantiomer **1b** is bound centrally between the 5′-AATT base pair sequence. Pyr^+ and Am^+ represent the positively charged 2-amino-1-pyrrolinium and amidinium groups of the drug, respectively. The dots labeled in the lexitropsin close to Am^+ and Pyr^+ represent H12 and H7, respectively.

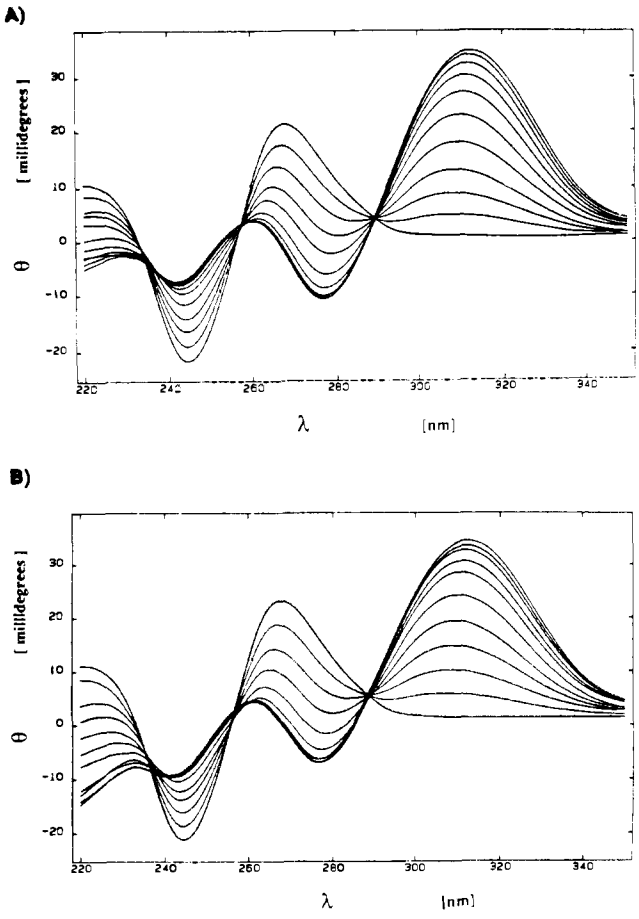

Figure 10. CD titration of poly[d(AT)]·poly[d(AT)] (1.81×10^{-4} M) with the enantiomers (4*S*)-**1a** and (4*R*)-**1b** in 10 mM sodium phosphate and 1 mM EDTA buffer at 298 K and pH 7.00: (A) binding-induced CD spectra of (4*S*)-**1a** enantiomer at different values of *n*(ligand)/*n*(base pairs); (B) binding-induced CD spectra of (4*R*)-**1b** enantiomer at different values of *n*(ligand)/*n*(base pairs).

proceeds without a change in the chemical environment of the drug since there is no doubling of resonances for the drug pyrrole protons. This observation would rule out any form of sliding of the drug along the DNA during the exchange process. In addition, all five sets of imino proton NMR signals of both complexes can

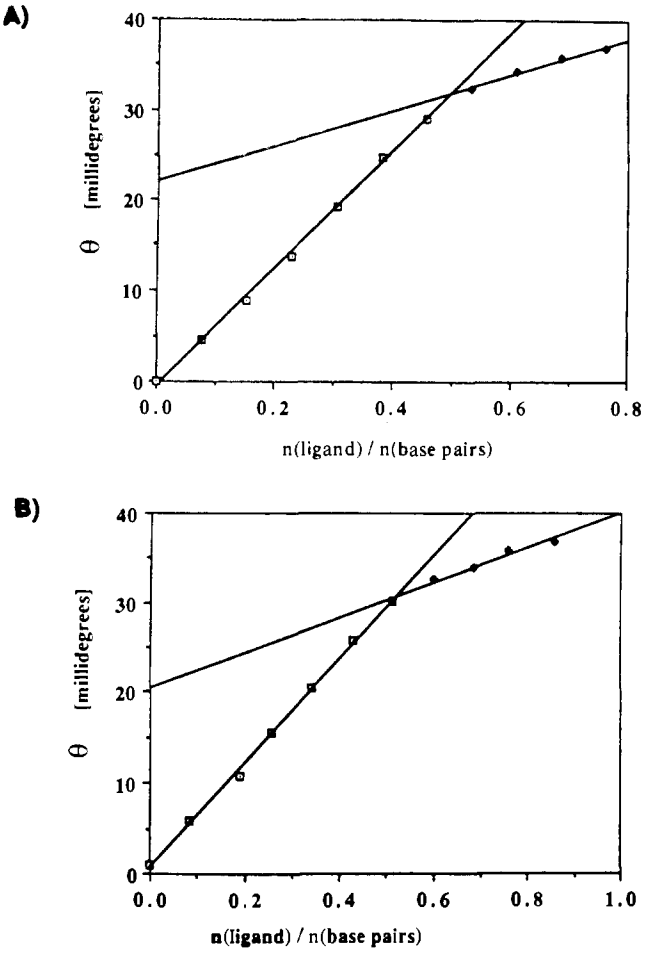

Figure 11. (A) Binding-induced ellipticity of (4*S*)-**1a** enantiomer at 310 nm as a function of *n*(ligand)/*n*(base pairs); (B) binding-induced ellipticity of (4*R*)-**1b** enantiomer at 310 nm as a function of *n*(ligand)/*n*(base pairs).

be detected at 21 °C. These results indicate that the duplex DNA must be stabilized by the binding of the drugs and exchange of the imino protons to the medium is slowed down. Therefore, the exchange of **1a** and **1b** on the equivalent 5′-AATT sites of the DNA in complex A (Figure 9A) and complex B (Figure 9B) is likely to proceed via a flip-flop mechanism without dissociation of the ligand from the DNA.

CD Spectroscopy. Figure 10A,B shows the two families of CD curves that result when (4*S*)-**1a** and (4*R*)-**1b** are titrated into solutions of poly[d(AT)]·poly[d(AT)]. The discrete isoelliptic points near 289, 259, and 236 nm suggest that only one type of binding occurs for each drug. Figure 11A,B shows the corresponding binding curves derived for each drug from the CD data. The discontinuities in these curves were used to define the binding site size associated with each drug at saturation. These data are listed in Table II along with the corresponding thermodynamic binding profiles.

Salt Dependence of Binding. Figure 12 shows ln–ln plots that illustrate the salt dependence of the binding constants for the complexation of (4*S*)-**1a** and (4*R*)-**1b** with the poly[d(AT)]·poly[d(AT)] duplex. Both plots are linear and exhibit similar slopes ($\partial \log K_b/\partial \log [Na^+]$) of 0.81 for (4*S*)-**1a** and 0.87 for (4*R*)-**1b**. These data are listed in Table II. The magnitude of the salt-dependent data ($\partial \log K_b/\partial \log [Na^+]$) primarily reflects the contributions that electrostatic interactions make to the DNA binding event of each drug.[24f-h] Thus, the similar slopes of 0.81 and 0.87 for the binding of (4*S*)-**1a** and (4*R*)-**1b** to poly[d(AT)]·poly[d(AT)] reflect nearly equal electrostatic contributions to the DNA binding of these two optical isomers. This result suggests that the subtle differences in binding interactions revealed by the NMR studies on the $d(CGCAATTGCG)_2$ complex of these

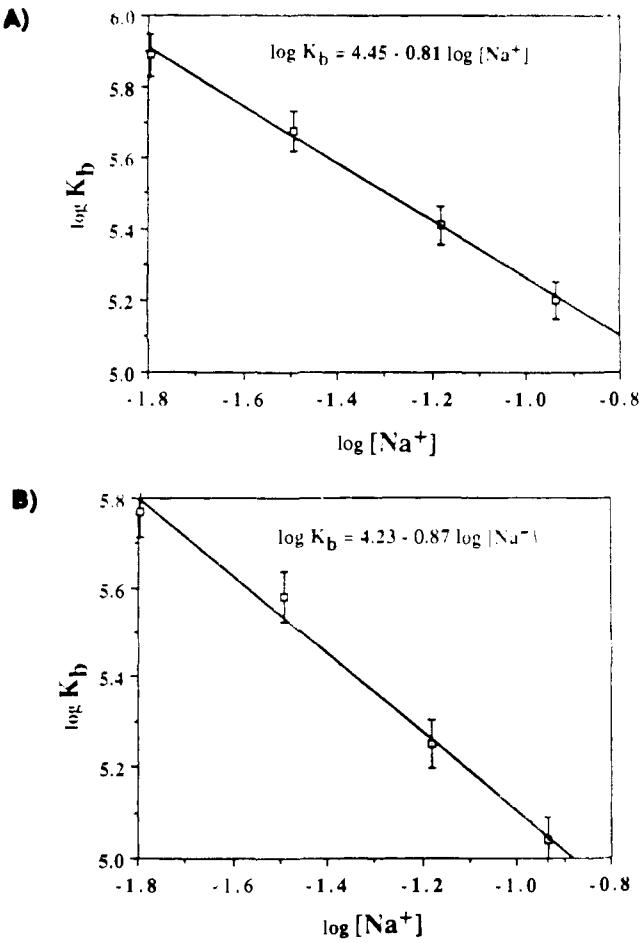

Figure 12. Salt dependence of the equilibrium binding constant, K_b, for the association of (A) enantiomer (4*S*)-**1a** and (B) enantiomer (4*R*)-**1b** to the poly[d(AT)]·poly[d(AT)] duplex at 298 K. Salt added, NaCl; solvent, 10 mM sodium phosphate and 1 mM EDTA buffer; pH 7.00. Error bars are indicated.

two drugs do not alter the overall electrostatic contributions to binding.

Further insight can be derived by examining the magnitude of the (∂ log K_b/∂ log [Na^+]) derivative. This derivative is equal to 1.76 for the binding of divalent cations to B-form DNA duplexes.[24g,h] However, inspection of the data in Table II reveals (∂ log K_b/∂ log [Na^+]) values that are close to 0.8 for both dicationic ligands. Thus, despite their formal dicationic nature, the DNA binding of both optical isomers exhibit salt dependencies that are more characteristic of monocations than of dications

Binding Enthalpies. Batch calorimetry was used to measure the enthalpy change associated with the binding of each enantiomer to the poly[d(AT)]·poly[d(AT)] host duplex. The resulting binding enthalpies, $\Delta H°$, are listed in Table II along with the corresponding value for netropsin. Inspection of these data reveals that both enantiomers exhibit very similar binding enthalpies. Thus, the stereochemical difference between (4*S*)-**1a** and (4*R*)-**1b** does not alter the overall enthalpy of interaction with poly[d(AT)]·poly[d(AT)]. However, the enantiomers exhibit binding enthalpies that are substantially less exothermic than the binding enthalpy of netropsin, a structurally similar ligand. This result suggests that relatively minor alterations in the structure of a ligand can have a profound effect on its binding enthalpy.

Binding Thermodynamics. Using a combination of the spectroscopic and calorimetric techniques described in the Experimental Section, we have determined complete thermodynamic profiles ($\Delta G°$, $\Delta H°$, $\Delta S°$) for the binding of each anthelvencin enantiomer [(4*S*)-**1a** and (4*R*)-**1b**] to the poly[d(AT)]·poly[d(AT)] host duplex. For each binding event, we also have determined the salt dependence of the equilibrium constant (∂ log K/∂ log [Na^+]). These thermodynamic and extrathermodynamic data are summarized in Table II. For comparative purposes, we have also included the corresponding data for netropsin binding to the poly[d(AT)]·poly[d(AT)] duplex.[24e]

Discussion

Structurally, anthelvencin is closely related to netropsin. Both are tripeptides that are similar in length and possess two cationic charges. However, in anthelvencin the guanidinium side chain of netropsin has been replaced with a 2-amino-1-pyrrolinium group, which is attached to a pyrrole moiety. The fact that the pyrrole is lacking an *N*-methyl substituent raises the possibility that the pyrrole N–H of anthelvencin can participate in hydrogen bond donation to sites on DNA.

As is evident from the DNase I footprinting studies, both isomeric anthelvencins bind to identical DNA sites. Inspection of the autoradiographic data revealed that the sites that initially bind ligand have four contiguous A·T base pairs, i.e., $(A·T)_4$. Weaker sites, which can be seen in the region 101–83 on the fragment, are four nucleotides in length but they possess a single G·C base pair, i.e., $(A·T)_3(G·C)$. This behavior, identical with that of netropsin, strongly suggests that both compounds possess similar if not identical binding modes toward DNA. Thus, the three amide hydrogens of anthelvencin are expected to be involved in bifurcated hydrogen bonds to adenine-N3 and thymine-N2. As is supported by the NMR data, the sequence-reading process involves close contacts between the pyrrole hydrogens H7 and H12 and adenine hydrogen on C2. This indicates that although anthelvencin has the structural option of directing the pyrrole N–H toward DNA, this does not occur. This would force the loss of a hydrogen bond between the amide located on the amino terminus of the dipeptide and DNA and potentially replace it with a new hydrogen bond between the pyrrole and DNA. Apparently, the remaining hydrogen bond and van der Waals contacts present in the ligand–DNA interface make this hydrogen bond exchange energetically unfavorable and it does not occur.

The DNase I footprinting studies indicate only weak stereoselectivity of the enantiomeric anthelvencins upon binding to DNA. Indications of a slight preference for binding of the natural (4*S*)-(+)-**1a** with DNA compared with (4*R*)-(−)-**1b** are also obtained from ethidium displacement[18] and are corroborated by the ^1H NMR data. The results of the calorimetric studies for the enantiomeric anthelvencins and a comparison with netropsin are summarized in Table II. These show that the enantiomeric anthelvencins exhibit substantially lower binding affinities ($\Delta G°$) than netropsin. Therefore, since all three ligands are bis-cationic, the shape and conformation of the amino-terminus cationic group significantly affects the efficiency of binding, while chirality of such terminal groups has less effect. The observed low stereoselectivity sharply contrasts with that of two enantiomeric dihydroxybis(netropsin)succinamides recently studied by Griffin and Dervan.[33] Since the succinamides possess two chiral centers positioned between two strong nonchiral DNA binding groups (netropsin), the chiral recognition element is "forced" to contact DNA sites, thereby enhancing stereoselectivity. This is not the case with anthelvencin where the chiral center is located at the terminus of the peptide chain in a region of greater conformational freedom.

The NMR studies reveal subtle differences in the binding of the enantiomeric anthelvencins. The studies reveal that the N to C termini of both enantiomeric forms of anthelvencin A, (4*S*)-**1a** and (4*R*)-**1b**, bind to the sequence 5′-AATT-3′ of the DNA. NOE studies show that the (4*S*) enantiomer **1a** is propeller twisted between the two pyrrole moieties to provide structural flexibility for the drug to bind snugly in the minor groove along the 5′-AATT sequence on the DNA in accord with the footprinting studies. In contrast, the conformation of the (4*R*) enantiomer **1b** is closer to coplanar when bound to the DNA. It is also shown that the (4*S*) chirality of **1a**, with its H(4*S*) pointing out of the minor groove, is better suited for the favorable electrostatic interactions between the positively charged 2-amino-1-pyrrolinium group and the DNA. It is also demonstrated that the drug (4*S*)-**1a** is bound diagonally across the $d[(A_4A_5T_6T_7)·(A_4A_5T_6T_7)]$ DNA duplex

Table II. Thermodynamic Binding Profiles for the Association of the Enantiomers (4*S*)-**1a** and (4*R*)-**1b** with the Poly[d(AT)]·poly[d(AT)] Duplex and the Salt Dependence of Their Equilibrium Binding Constants at 298 K Compared with the Corresponding Values for Netropsin Binding to the Same DNA

ligand	B_h[a]	$\Delta H°$, kJ/mol	$\Delta G°$, kJ/mol	$\Delta S°$, J/mol-K	$\partial \log K_b/\partial \log [Na^+]$
netropsin[b]	0.25	−46.9	−53.1	20.9	−1.6
(4*S*)-**1a**	0.5	−9.6	−33.5	80.3	−0.81
(4*R*)-**1b**	0.5	−9.2	−33.0	79.5	−0.87

[a] B_h = number of binding sites/bases pair at saturation. [b] Reference 24e.

(see Figure 9A). In contrast, the unnatural enantiomer (4*R*)-**1b** behaves like achiral lexitropsins and binds centrally between the 5′-AATT sequence (see Figure 9B). The steric interaction between the (4*R*) proton on **1b** and the DNA interferes with the electrostatic attraction between the positively charged 2-amino-1-pyrrolinium group and the DNA. The exchange rate of (4*S*)-**1a** between the two equivalent 5′-AATT sites via the flip-flop mechanism is ~36 s^{-1} at 21 °C with $\Delta G^{\ddagger}$ of 68.3 ± 5 kJ mol^{-1}. In contrast, the (4*R*) enantiomer **1b** exchanges faster (77 s^{-1} at 21 °C) between the two equivalent binding sites than **1a**.

It is also demonstrated that the van der Waals interaction between the methylene protons (H18) of the C terminus of these drugs and the G-2-NH_2 group prevents binding to a 3′-terminal GC position and, by default, is responsible for reading of a 3′-dA·dT base pair in both complexes.[32] NOE measurements of the two complexes show that both DNA duplexes exist as right-handed helices of the B family, which are similar to the conformation of the free decadeoxyribonucleotide $d(CGCAATTGCG)_2$.[5] Therefore, binding of (4*S*)-**1a** and (4*R*)-**1b** to the DNA result in minimal conformational distortion.

Inspection of the data listed in Table II reveals the following significant features: The two enantiomers of anthelvencin exhibit nearly identical binding free energies. Thus, the stereochemical difference between the two enantiomers studied here does not significantly alter the binding affinity ($\Delta G°$) for the poly[d(AT)]·poly[d(AT)] duplex. This result is consistent with our DNase I footprinting data which reveal that the two optical isomers exhibit comparable levels of inhibition at identical ligand concentrations.

Netropsin binding to the poly[d(AT)]·poly[d(AT)] duplex exhibits a binding constant, K_b, that is 2×10^3 times greater than the corresponding binding constants for either anthelvencin enantiomer (2×10^9 versus $\sim 1 \times 10^6$). This large netropsin binding preference is entirely enthalpic in origin (−46.9 kJ/mol for the netropsin binding enthalpy versus −9.2 to −9.6 kJ/mol for the anthelvencin binding enthalpies). If we assume that netropsin and the anthelvencins exhibit similar DNA–drug interactions in the minor groove (a reasonable assumption based on a comparison of the NMR data), then our results suggest that relatively small alterations in drug structure can cause dramatic changes in the binding thermodynamics.[37]

The binding constants of both anthelvencin enantiomers exhibit nearly identical salt dependencies ($\partial \log K_b/\partial \log [Na^+] = 0.81$ and 0.87), thereby reflecting equal electrostatic contributions to the DNA binding of the two optical isomers. Thus, the stereochemical difference between the two enantiomers does not alter the overall electrostatic contribution to the DNA binding event. However, as noted earlier, the magnitude of the salt dependence is characteristic of monocationic binding despite the formal dicationic nature of both ligands. We have observed such behavior previously for the DNA binding of the dicationic steroid dipyrandium.[24b] Such a reduced electrostatic contribution for the DNA binding of a dicationic ligand may in part reflect shielding of one of the charges on the ligand due to structural differences between the two charged termini. Alternatively, the overall structure and/or conformation of the ligand may be such as to prevent both charge ends from simultaneously and efficiently interacting with the DNA host.

The manner in which ligand size, chiral location, and the specific nature of the chiral element influence stereoselectivity and sequence specificity is under active investigation in our laboratories.

Acknowledgment. This investigation was supported by grants to J.W.L. from the National Cancer Institute of Canada and the Biotechnology Strategic Grants program of the Natural Sciences and Engineering Research Council of Canada and to K.J.B. from the National Institutes of Health (GM-23509 and GM-34469) and the Johnson & Johnson Research Discovery Program. J.A.H. thanks the Alberta Heritage Foundation for Medical Research for a fellowship.

Registry No. 1a, 113598-28-0; **1b**, 113598-34-8; d(CGCAATTGCG), 111663-15-1.

Supplementary Material Available: Assignment of nonexchangeable ^1H NMR resonances in complexes A and B (3 pages). Ordering information is given on any current masthead page.

(37) At saturation, both anthelvencin enantiomers exhibit identical binding site sizes ($1/B_h$) of two base pairs per drug bound as determined from CD titration curves. This result should be compared with our footprinting and NMR data which suggest a binding site size of four base pairs for the anthelvencins (a value consistent with that derived for netropsin). This apparent disparity may reflect differences inherent in the three methods used to characterize the binding site size. Specifically, the optical titration curve provides a measure of the binding site size at maximum binding density (saturation). By contrast, the footprinting data define the binding site size as the DNA domain size that is protected from enzyme digestion at low binding densities (well below saturation). Furthermore, the NMR data were obtained at a 1:1 mol equiv of drug to DNA. Consequently, the first and the last methods may not necessarily yield comparable binding site sizes. In fact, a drug "bound" to only two base pairs may nevertheless inhibit enzyme cutting of adjacent phosphodiester bonds, thereby yielding an apparent binding site size of four base pairs in footprinting studies. Alternatively, for certain types of drugs, the binding density measured at saturation by Job plots may be different from the binding density measured at low drug to base pair ratios by using footprinting techniques. A class of drugs that might exhibit this type of behavior would have one terminus strongly bound and may even project away from the groove. Our data suggest that the anthelvencins may behave in this manner.